

# Near-field thermal upconversion through a Kerr medium

Chinmay Khandekar<sup>1</sup> and Alejandro W. Rodriguez<sup>1</sup>

*Department of Electrical Engineering, Princeton University, Princeton, NJ 08540*

(Dated: today)

We present an approach for achieving high-efficiency Kerr  $\chi^{(3)}$ -mediated thermal energy transfer at the nanoscale. Using a simple description of four-wave mixing processes based on coupled-mode theory, we study upconversion and transfer of thermal energy from mid- to near-infrared wavelengths in a configuration involving SiC and K slabs separated by a gap that is partially filled with a  $\chi^3$  nonlinear medium—a lattice of metallic particles embedded in GaAs. We show that when illuminated by externally incident, infrared light of relatively low  $\text{mW}/\mu\text{m}^2$  intensities and under suitable geometric parameters and conditions, it is possible to achieve and even exceed typical thermal flux rates in the near field. Such a scheme therefore provides a potential approach for achieving thermal cooling and refrigeration at the nanoscale.

Optical nonlinearities are inherently weak and are therefore rarely exploited in bulk media<sup>1</sup>. More commonly, they are strengthened by exploiting optical cavities such as large-etalon mirrors<sup>2</sup>, photonic-crystal defects<sup>3</sup> and plasmonic resonators<sup>4</sup>, that confine light over small mode volumes and long times<sup>5</sup>. As the power requirements of nonlinear devices are scaled down, even relatively small effects stemming from thermal fluctuations can be altered by material nonlinearities<sup>6,7</sup>, but such phenomena have only just recently begun to be explored<sup>8,9</sup>. In recent work, we showed that at high temperatures, optical nonlinearities can have a significant impact on thermal emission from photonic resonators, leading for instance to highly modified lineshapes<sup>8</sup> and thermally activated transitions<sup>10</sup>. In this letter, we show that the Kerr  $\chi^{(3)}$  nonlinear response of a passive medium can be exploited to upconvert thermal energy “trapped” in the near field of a planar body from mid- to near-infrared wavelengths. Our predictions are based on a coupled-mode theory (CMT) framework<sup>16</sup> of resonant four-wave mixing processes that provides general geometric and operating conditions needed to maximize upconversion. In particular, we consider a proof-of-concept system consisting of silicon carbide (SiC) and potassium (K) slabs separated by a small gap containing a  $\chi^{(3)}$  medium—an array of metallic particles embedded in gallium arsenide (GaAs). In the near field, i.e. short gap sizes  $\ll$  thermal wavelength  $\lambda_T \approx 10\mu\text{m}$  near room temperature, bound slab surface-resonances contribute heat and lead to thermal flux rates greatly exceeding those of blackbodies in the far field<sup>11</sup>. We show that when illuminated by infrared light of relatively low intensities  $\sim \text{mW}/\mu\text{m}^2$ , the intervening medium mediates large upconversion and transfer of heat from the SiC to K slab. Our predictions extend recent work exploring the role of active media in extracting thermal energy in the near field<sup>17–19</sup> and provide an avenue for achieving thermal refrigeration.<sup>19–21</sup>

We first illustrate the basic thermal upconversion mechanism by considering a representative system, depicted in the top inset of Fig. 1(a), involving resonators that support modes at  $\omega_1$ ,  $\omega_2$ , and  $\omega_3 = \omega_1 + 2\omega_2$ , the second of which is coupled to an external channel. The modes are assumed to have widely different frequency

and therefore do not couple linearly to one another. They can however interact nonlinearly through a four-wave mixing process<sup>1</sup> mediated by a  $\chi^{(3)}$  medium via their field  $E_j$  ( $j = 1, 2, 3$ ) overlaps and initiated by externally incident light at  $\omega_2$  from the channel. Such a system is well described by the temporal CMT framework in terms of a few key geometric parameters.<sup>16</sup> Since typical pump energies tend to be much greater than the available thermal energy at  $\omega_{1,3}$ , nonlinear mixing in this system simplifies under the undepleted-pump approximation<sup>22</sup> and is well described by the following linear equations:

$$\frac{da_1}{dt} = (i\omega_1 - \gamma_1)a_1 - i\kappa e^{-2i\omega_2 t} a_3 + \sqrt{2\gamma_{1d}}\xi_1 \quad (1)$$

$$\frac{da_3}{dt} = (i\omega_3 - \gamma_3)a_3 - i\frac{\omega_3}{\omega_1}\kappa^* e^{2i\omega_2 t} a_1 + \sqrt{2\gamma_{3d}}\xi_3 \quad (2)$$

where  $a_j$  denotes the mode amplitude of mode  $j \in [1, 3]$ , normalized so that  $|a_j|^2$  is the mode energy, and  $\gamma_j = \gamma_{jd} + \gamma_{jc}$  denotes its decay rate, resulting from either material dissipation  $\gamma_{jd}$  or coupling to external channels  $\gamma_{jc}$  (e.g. radiation or a waveguide). Each mode is assumed to be in local thermodynamic equilibrium<sup>8</sup> and hence subject to thermal sources  $\xi_j$  satisfying  $\langle \xi_j^*(\omega)\xi_j(\omega') \rangle = \Theta(\omega, T_j)\delta(\omega - \omega')$ , where  $\Theta(\omega, T_j) = \hbar\omega / [\exp(\hbar\omega/k_B T_j) - 1]$  is the Planck distribution associated with the local resonator temperature  $T_j$  and  $\langle \dots \rangle$  denotes a thermodynamic, ensemble average.<sup>23</sup> Here, thanks to the undepleted-pump approximation, the otherwise nonlinear role of the pump is captured instead by a *linear* coupling coefficient given by:

$$\kappa = \frac{2\beta\omega_1\gamma_{2c}P}{\gamma_2^2}, \quad (3)$$

where  $P$  denotes the monochromatic power incident from the channel and  $\beta$  is a nonlinear coupling coefficient,

$$\beta = \frac{\int dV \chi_{ijkl}^{(3)}/\epsilon_0 E_{1i} E_{2j} E_{2k} E_{3l}^*}{\sqrt{\int dV \frac{\partial(\omega\epsilon)}{\partial\omega} E_{1i}^* E_{1i} \int dV \frac{\partial(\omega\epsilon)}{\partial\omega} E_{3i}^* E_{3i} \int dV \frac{\partial(\omega\epsilon)}{\partial\omega} E_{2i}^* E_{2i}}},$$

that depends on a spatial overlap of the linear cavity fields  $E_{ji}$  over the (generally anisotropic) susceptibility

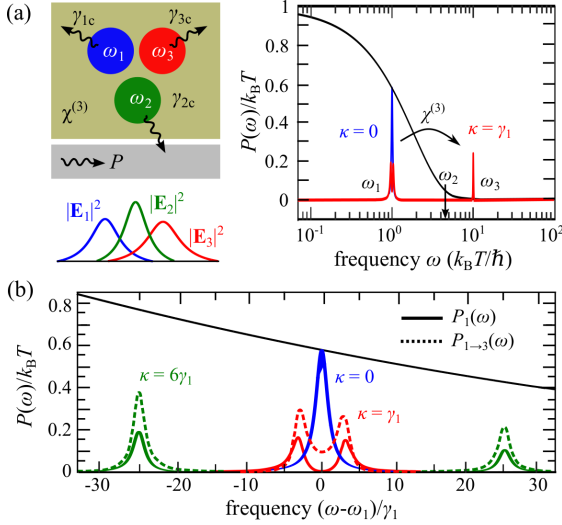


FIG. 1. (a) Schematic of three equal-temperature  $T$  resonators supporting modes at  $\omega_1 = k_B T / \hbar$ ,  $\omega_2 = 1/2(\omega_3 - \omega_1)$ , and  $\omega_3 = 10\omega_1$ , each decaying with decay rate  $\gamma_j$  due to internal dissipation  $\gamma_{jd}$  and/or coupling to an external channel  $\gamma_{jc}$  (radiation or a waveguide), with  $\gamma_{jd} = \gamma_{jc} = 0.01\omega_1$ , for  $j = \{1, 2, 3\}$ . Thermal modes 1 and 3 are strongly coupled through a four-wave mixing process mediated by a Kerr  $\chi^{(3)}$  medium (light green) and incident light from the waveguide of power  $P$  and frequency  $\omega_2$ . As argued in the text, nonlinear mixing between modes 1 and 3 can be described by an effective, linear but power-dependent coupling  $\kappa$  [Eq. (3)]. (b) Thermal emission spectrum  $P(\omega)$  (blue and red curves) of the system, normalized by  $k_B T$ , as a function the dimensionless frequency  $\hbar\omega/k_B T$ . Emission at any  $\omega$  is bounded by the Planck distribution  $\Theta(\omega, T)$  (black curve) in the absence of the pump  $\kappa = 0$  (blue curves) but can be exponentially enhanced under finite  $\kappa > 0$  (red curves). (c) Thermal emission  $P_1(\omega)$  (solid lines) and heat-transfer  $P_{1 \rightarrow 3}(\omega)$  (dotted lines) spectra near  $\omega_1$  as a function of the dimensionless frequency  $(\omega - \omega_1)/\gamma_1$ , demonstrating splitting of the resonances into Stokes (red-shifted) and anti-Stokes (blue-shifted) peaks which grows with increasing  $\kappa$  and further enhances emission.

$\chi_{ijkl}^{(3)}$  of the nonlinear medium. The indices  $j \in [1, 2, 3]$  and  $i \in [x, y, z]$  run over the mode number and cartesian components of the mode profiles, while  $\epsilon_0$  and  $\epsilon$  denote the vacuum and relative permittivity of the system. Note that in addition to frequency mixing, the Kerr nonlinearity will also lead to additional, cross-phase modulation terms<sup>1</sup> that shift the resonator frequencies and hence disturb the frequency-matching condition  $\omega_3 = \omega_1 + 2\omega_2$ .<sup>22,24</sup> Below, we account for all possible sources of frequency mismatch, e.g. geometric and material dispersion or fabrication imperfections, by introducing a frequency offset  $\Delta\omega$  in the incident light.

The linearity of the coupled-mode equations allows for the heat-transfer  $P_{1 \rightarrow 3} = \langle 2 \text{Im}[\kappa \exp(2i\omega_2 t) a_3^* a_1] \rangle$  and thermal-radiation  $P_j = 2\gamma_{jc} \langle |a_j|^2 \rangle$  flux rates to be expressed in closed form, leading to the following power

spectral densities:

$$P_{1 \rightarrow 3}(\omega) = \frac{4|\kappa|^2}{D_1(\omega)} [-\gamma_1 \gamma_{3d} \Theta(\omega + 2\omega_2, T_3) + \gamma_{1d} \gamma_3 (\omega_3/\omega_1) \Theta(\omega, T_1)] \quad (4)$$

$$P_1(\omega) = \frac{4\gamma_{1c}}{D_1(\omega)} [\gamma_{1d} |i(\omega - \omega_1 - \Delta\omega) + \gamma_1|^2 \Theta(\omega, T_1) + \gamma_{3d} |\kappa|^2 \Theta(\omega + 2\omega_2, T_3)] \quad (5)$$

$$P_3(\omega) = \frac{4\gamma_{3c}}{D_3(\omega)} [\gamma_{3d} |i(\omega - \omega_3 + \Delta\omega) + \gamma_3|^2 \Theta(\omega, T_3) + \gamma_{1d} (\omega_3/\omega_1) |\kappa|^2 \Theta(\omega - 2\omega_2, T_1)] \quad (6)$$

where  $D_1(\omega) = |(i(\omega - \omega_1) + \gamma_1)(i(\omega - \omega_1 - \Delta\omega) + \gamma_3) + \omega_3 |\kappa|^2 / \omega_1|^2$  and  $D_3 = D_1(1 \leftrightarrow 3, \Delta\omega \rightarrow -\Delta\omega)$ . These simple expressions capture the most important features of the system. Consider for instance the particular scenario of equal-temperature  $T$  cavities with  $\omega_1 = k_B T / \hbar$ ,  $\omega_3 = 10\omega_1$ ,  $\gamma_{jd} = \gamma_{jc} = 0.01\omega_1$ , and  $\Delta\omega = 0$ , such that the resonators exhibit the largest possible emissivities  $\varphi_j \equiv P_j / \Theta(\omega_j, T)$  in the absence of the pump (blue curves). Figure 1(a) shows the system's thermal radiation spectrum near the resonances under finite  $\kappa = \gamma_1$  (red curves), revealing huge enhancements in  $\varphi_3 \gg 1$  stemming from the transfer of thermal energy from  $\omega_1$  to frequencies  $\omega_3 \gg k_B T / \hbar$  which are otherwise exponentially suppressed by the Planck distribution (black curve). Furthermore, Fig. 1(b) plots  $P_1(\omega)$  and  $P_{1 \rightarrow 3}(\omega)$  near  $\omega_1$ , illustrating that the pump also has a significant impact on the thermal lineshapes, causing the modal frequencies to split into Stokes ( $-$ ) and anti-Stokes ( $+$ ) peaks,  $\omega_1^\pm = \omega_1 + \frac{\Delta\omega \pm \sqrt{\Delta\omega^2 + 4(\gamma_1 \gamma_3 + \omega_3/\omega_1 |\kappa|^2)}}{2}$  and  $\omega_3^\pm = \omega_3^\pm(1 \leftrightarrow 3, \Delta\omega \rightarrow -\Delta\omega)$ , that grow apart with increasing  $\kappa$ . In addition to mediating energy transfer, the pump-induced red shift allows the resonator to effectively draw additional energy available at longer wavelengths from the Planckian reservoir, thus increasing its emission rate. In particular, the largest possible emission rate associated with the Stokes mode  $\varphi_3^{\text{max}} = k_B T / \Theta(\omega_3, T)$  occurs in the (unrealistic) limit of ultra-strong coupling  $\kappa \gg \gamma_{1,3}$ , perfect frequency and rate matching,  $\Delta\omega = 0$  and  $\gamma_1 = \gamma_3$ , and in the absence of spurious losses  $\gamma_{1c} = \gamma_{3d} = 0$ . The maximum achievable transfer rate  $P_{1 \rightarrow 3}^{\text{max}} = 2\gamma_{1d} k_B T$  occurs under similar conditions, except that thermal excitations at  $\omega_1$  must be upconverted and reabsorbed at  $\omega_3$  at a faster rate than they decay in resonator 1, achieved in the limit of  $|\kappa| \gg \gamma_3 \gg \gamma_1$ . While such a strong-coupling limit typically renders CMT invalid<sup>16</sup>, as we show below it is possible to observe significant splitting and flux enhancements in situations where CMT is still accurate, i.e.  $\kappa \gtrsim \gamma_j$  and  $\Delta\omega \lesssim \gamma_j, \kappa$ .

We now propose a practical implementation of this scheme in which coherent infrared light mediates transfer of thermal energy from a planar medium unto another. In particular, the inset of Fig. 2(b) depicts a geometry comprising SiC and K slabs of permittivities  $\epsilon_1$  and  $\epsilon_3$ , respectively, separated by a gap of size  $d$  that is filled (or

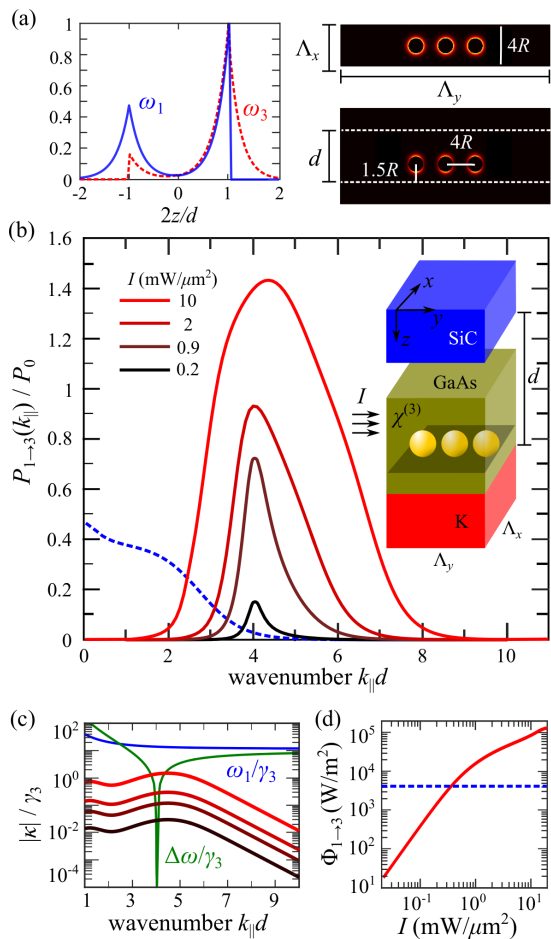


FIG. 2. Upconversion scheme involving a system (inset) of SiC and K slabs separated by a gap of size  $d = 100\text{nm}$  that is partially filled with a Kerr  $\chi^{(3)}$  nonlinear medium (GaAs). Embedded in the medium is a rectangular lattice of metallic particles with radius  $R = 15\text{nm}$ , lattice dimensions  $\Lambda_x \times \Lambda_y$ , where  $\Lambda_x = 5R$  and  $\Lambda_y = \pi c/\omega_2$ , and low in-plane filling fraction,  $f = 3\pi R^2/\Lambda_x \Lambda_y \approx 0.06$ . SiC and K surface-plasmon resonances at frequencies  $\omega_1$  and  $\omega_3$ , respectively, couple to dipolar particle-resonances at  $\omega_2 \approx 1/2(\omega_3 - \omega_1)$  that are excited by an incident, monochromatic,  $\hat{z}$ -polarized planewave of frequency  $\omega_2$  and intensity  $I$ . (a) Normalized planar mode profiles at a representative wavenumber  $k_{\parallel}d = 4$  along with energy-density contour plots ( $x$ - $y$  and  $y$ - $z$  cross sections) of the particle resonances, with yellow/black denoting maximum/zero amplitude. Marked in white are various lattice parameters and planar interfaces (white dashed lines). (b) Frequency-integrated heat-transfer spectrum  $P_{1 \rightarrow 3}(k_{\parallel})$ , normalized by  $P_0 = 2\gamma_1\Theta(\omega_1, T)$ , as a function of  $k_{\parallel}d$  and for multiple intensities  $I$ . (c) Variation of the coupling  $\kappa$ , frequency mismatch  $\Delta\omega$ , and frequency  $\omega_1$ , with respect to  $k_{\parallel}d$ . (d) Total heat-transfer rate per unit area  $\Phi_{1 \rightarrow 3}$  as a function of  $I$ . Also shown are the spectrum and flux rate (dashed blue lines) corresponding to semi-infinite SiC slabs separated by a vacuum gap but subject to a 300K temperature difference.

partially filled) with a nonlinear medium; the entire system is held at room temperatures,  $T = 300\text{K}$ . The plates support mid- and near-infrared surface-propagating plas-

mons characterized by transverse momenta  $\mathbf{k}_{\parallel}$  and dispersion relations  $\omega_{1,3}(\mathbf{k}_{\parallel})$  satisfying,

$$e^{2k_z d} = \frac{(\varepsilon_1 k_{z2} - \varepsilon_2 k_{z1})(\varepsilon_3 k_{z2} - \varepsilon_2 k_{z3})}{(\varepsilon_1 k_{z2} + \varepsilon_2 k_{z1})(\varepsilon_3 k_{z2} + \varepsilon_2 k_{z3})}, \quad (7)$$

where  $k_{zj} = \sqrt{k_{\parallel}^2 - \varepsilon_j \omega^2/c^2}$  and  $k_{\parallel} = |\mathbf{k}_{\parallel}|$ . The nonlinear medium consists of an  $\Lambda_x \times \Lambda_y$  rectangular lattice of metallic particles (shaded region) embedded in a Kerr  $\chi^{(3)}$  medium of permittivity  $\varepsilon_2$ . The purpose of the lattice is threefold: First, it acts as a grating that allows  $z$ -propagating incident light  $\propto \hat{z}e^{-i(k_{2y} + \omega_2 t)}$ , with  $k_2 = \sqrt{\varepsilon_2 \omega_2^2/c^2}$ , to couple to a given lattice Bloch mode. Second, Mie resonances at  $\omega_2$  designed by a judicious choice of particle sizes and shapes enhance the pump field and hence coupling coefficient  $\kappa$ . Third, it provides degrees of freedom with which to enforce ‘‘quasiphase matching’’ (below) over a broad range of  $k_{\parallel}$ .

The metal particles are assumed to have small radius  $R \ll 2\pi/k_2$ , allowing their plasmonic response to be treated within a quasistatic, dipolar approximation<sup>26</sup>. They are also placed far apart from one another, mitigating many-body scattering effects and allowing the induced field to be conveniently expressed as a linear superposition  $\sum_p E_2(\mathbf{x}_{\parallel} - \mathbf{x}_p, z)e^{-ik_2 y}$  of the isolated particle resonances, where  $\mathbf{x}_{\parallel}$  and  $\mathbf{x}_p$  denote the transverse coordinates and center of each particle and  $E_2(\mathbf{x}_{\parallel} - \mathbf{x}_p, z)$  denotes its mode profile. The  $p$ -polarized field profiles of the planar resonances are given by  $E_{j\ell}(z)e^{i\mathbf{k}_{\parallel, j} \cdot \mathbf{x}_{\parallel}}$ , with  $j = 1, 3$  and  $\ell \in \{x, y, z\}$ , in which case the nonlinear coupling coefficient  $\beta$  of each pair of modes is given by:

$$\beta \sim \sum_p \int dV \chi_{ijkl}^{(3)} e^{i(\mathbf{k}_{\parallel, 3} - \mathbf{k}_{\parallel, 1}) \cdot \mathbf{x}_{\parallel} + 2ik_2 y} \times E_{1i}(z)E_{2j}(\mathbf{x}_{\parallel} - \mathbf{x}_p, z)E_{2k}(\mathbf{x}_{\parallel} - \mathbf{x}_p, z)E_{3\ell}^*(z) \quad (8)$$

Here, the sum is taken with respect to the index  $p$  of each particle,  $\{i, j, k, \ell\}$  denote cartesian field components, and  $\chi_{ijkl}^{(3)}$  is the Kerr tensor of the background medium, assumed to be isotropic for convenience.

In order to take advantage of the large density of states available in the near field, we choose geometric and material parameters that ensure large  $\beta$  for a wide range of  $k_{\parallel}$ , known as quasiphase matching.<sup>27</sup> Here, we focus on modes having equal momentum  $\mathbf{k}_{\parallel} = \mathbf{k}_{\parallel, 1} = \mathbf{k}_{\parallel, 3}$ , in which case the integral in Eq. (8) no longer exhibits a wavevector-dependent phase factor. Our choice of a  $z$ -polarized incident wave simplifies matters further because cylindrically symmetric pump fields  $E_{2j}(\mathbf{x}_{\parallel} - \mathbf{x}_p, z)$  yield the same coupling coefficients irrespective of the propagation direction. More importantly, for any given mode pair, the overlap integral in Eq. (8) involves a sum over all particle positions, which vanishes unless the individual unit-cell contributions add constructively, guaranteed by an appropriate choice of period  $\Lambda_y = \pi/k_2$ . Although the lack of a ‘‘Bloch phase’’ in the  $\hat{x}$  direction means that at least in principle  $\Lambda_x$  can be much

smaller than  $\Lambda_y$ , here we choose  $\Lambda_x = 5R$  so as to ignore many-body effects on the induced field. Finally, since  $R \ll \Lambda_x, \Lambda_y$ , the unit cell [Fig. 2(a)] can be populated with multiple particles, distributed so as to maximize  $\beta$ .

Momentum-matched modes simplify the calculation of  $\beta$  but typically will not automatically satisfy the frequency-matching condition,  $\Delta\omega(k_{\parallel}) = \omega_3(k_{\parallel}) - \omega_1(k_{\parallel}) - 2\omega_2 \lesssim \gamma_j, \kappa$ , which is primarily determined by the choice of materials. Here we consider typical materials,<sup>1,28–33</sup> choosing GaAs as the intermediate nonlinear medium due to its relatively large Kerr coefficient,  $\chi^{(3)} \approx 1 \times 10^{-18} \text{m}^2/\text{V}^2$ . We also explore one of several possible tuning mechanisms typically employed to ensure frequency matching<sup>27</sup>, relying on the choice of particle size and material dispersion to engineer  $\omega_2$ .<sup>34,35</sup> As a proof of concept, we choose particles of radius  $R = 15\text{nm}$  with optical properties described by a Drude model of plasma frequency  $\omega_p = 3.2 \times 10^{15} \text{rad/s}$  and decay rate  $\gamma_p = 0.002\omega_p$ , leading to a resonance frequency  $\omega_2 = 6.68 \times 10^{14} \text{rad/s}$  and dissipative and radiative decay rates,  $\gamma_{2d} = 2.26 \times 10^{11} \text{rad/s}$  and  $\gamma_{2c} = 1 \times 10^{11} \text{rad/s}$ , respectively. Assuming incident light of intensity  $I$ , the power per sphere, i.e. the quantity entering the CMT, is given by  $P = \frac{\omega_2}{\gamma_{2c}} \pi R^2 I$ .<sup>26</sup> This choice of materials results in lattice parameters  $\Lambda_x = 5R = 75\text{nm}$  and  $\Lambda_y = \pi c/\omega_2 = 426\text{nm}$ . Note that the impact of the metal particles on the planar dispersions, obtained via the complex-frequency solutions of Eq. (7), is negligible owing to their relatively low in-plane filling fraction  $f = \frac{3\pi R^2}{\Lambda_x \Lambda_y} \approx 0.06$  and to their off-resonant response at the vastly different planar resonance frequencies. Figure 2(a) shows typical mode profiles at a representative  $k_{\parallel} = 4/d$ , with the large peak near the GaAs–K interface motivating our choice of lattice center [Fig. 2(a)].

Given the coupled-mode parameters, the heat transfer rate  $P_{1 \rightarrow 3}(k_{\parallel}) = \int_0^{\infty} \frac{d\omega}{2\pi} P_{1 \rightarrow 3}(\omega, k_{\parallel})$  at each  $k_{\parallel}$  can be obtained by integrating Eq. (4) over all  $\omega$ , leading to the following expression for the total flux per unit area:<sup>36,37</sup>

$$\Phi_{1 \rightarrow 3} = \frac{1}{2\pi} \int_0^{\infty} dk_{\parallel} k_{\parallel} P_{1 \rightarrow 3}(k_{\parallel}).$$

Figure 2(b) shows the ratio of  $P_{1 \rightarrow 3}(k_{\parallel})$  to the thermal radiation rate of an isolated thermal resonance  $P_0 = 2\gamma_1 \Theta(\omega_1, T_1)$ , as a function of the dimensionless wavenumber  $k_{\parallel}d$  for  $d = 100\text{nm}$  and increasing intensity  $I$  (from black to red). Figure 2(c) shows the associated variations in the coupling  $|\kappa|$ , frequency mismatch  $\Delta\omega$ , and plasmon frequency  $\omega_1$ , all normalized by  $\gamma_3$ . We assume typical values of  $\gamma_1 \approx 4.48 \times 10^{11} \text{rad/s}$  and  $\gamma_3 \approx 1.3 \times 10^{13} \text{rad/s}$ . As shown, the spectrum exhibits a small peak at  $k_{\parallel}d \approx 4$  that grows and widens with increasing  $I$ , causing the overall flux per unit area  $\Phi_{1 \rightarrow 3}$ , plotted in Fig. 2(d), to monotonically increase and eventually saturate as  $I \rightarrow \infty$ . These features are explained as follows: First, Eq. (4) shows that in the weak coupling regime  $|\kappa|/\gamma_3 \ll 1$ , the flux rate  $\Phi_{1 \rightarrow 3} \sim |\kappa|^2 \sim I^2$ . Second, Fig. 2(c) shows that the bandwidth of the spectrum

is primarily determined by the range of modes satisfying the frequency matching constraint  $\Delta\omega \lesssim \gamma_j, |\kappa|$ , with the peak occurring at the value of  $k_{\parallel}$  that minimizes  $\Delta\omega$ . At small  $I$  or equivalently,  $\kappa/\gamma_3 \ll 1$ , the range of modes satisfying  $\Delta\omega \lesssim \gamma_3$  is narrow, with higher intensities increasing  $\kappa$  and hence allowing frequency matching to be satisfied over a wider range of  $k_{\parallel}$ . Third, the rapid decrease in the flux rate at large  $k_{\parallel}d \gg 1$  stems from the fact that  $\beta$  and hence  $\kappa$  depends on the spatial decay of the planar mode profiles, which decrease exponentially with increasing  $k_{\parallel}$ . We remark that the precise value of  $k_{\parallel}$  at which  $\Delta\omega(k_{\parallel}) = 0$  depends primarily on the particle resonance frequency: although its occurrence at larger  $k_{\parallel}$  would facilitate increased bandwidths due to the lack of dispersion at large  $k_{\parallel} \gg \omega/c$ , the resulting exponential suppression in  $\beta$  suggests instead an optimal choice of particle parameters for a given  $d$ , here chosen to be an intermediate  $k_{\parallel}d \approx 4$ . Note also that we only consider  $\Delta\omega$  arising from material dispersion and ignore power-dependent shifts due to cross-phase modulation,<sup>22</sup> which tend to be small and in any case can be compensated by suitable lattice parameters. Finally, as discussed above, the ratio  $P_{1 \rightarrow 3}/P_0$  can exceed one when the system enters the strong coupling regime  $\gamma_3 \lesssim |\kappa| \ll \omega_1$ , in which case the Stokes peak can draw additional thermal energy available at longer wavelengths.

For comparison, Figs. 2(b) and (d) also show the flux rates associated with identical SiC plates separated by a vacuum gap and maintained at  $T = 300\text{K}$  and  $0\text{K}$ , computed via the well-known fluctuational electrodynamics framework in terms of the reflection coefficients of the slabs.<sup>11</sup> Compared to  $P_{1 \rightarrow 3}$ , the exponential decay of the spectrum in this typical scenario occurs at smaller  $k_{\parallel}d \approx 1$ <sup>37</sup>, the reasons behind which are twofold: First, the increased proximity of Mie resonances to planar interfaces leads to slightly larger mode overlaps. Second and most importantly,  $\kappa$  increases with  $I$  and thus allows thermal energy in the SiC to be upconverted and absorbed at a faster rate  $\kappa \gg \gamma_1$  than it is dissipated. When combined with the aforementioned Stokes enhancement, the net effect is a significant increase in the nonlinear flux rate, which overcomes its linear counterpart  $\approx 10^4 \text{W}/\text{m}^2$  at a threshold intensity  $I \approx 0.3\text{mW}/\mu\text{m}^2$ . Finally, we remark that while heat extraction in the passive scenario requires  $T_1 > T_3$ , it follows from Eq. (4) that in the nonlinear case, the SiC slab will be cooled so long as  $\omega_3 \Theta(\omega_1, T_1) > \omega_1 \Theta(\omega_3, T_3)$ . Such a refrigeration mechanism allows external work performed by the coherent pump to carry heat from a cold to a hot body, with pump-induced heating potentially mitigated by exploiting semi-transparent slabs at  $\omega_2$ , which is the case here.

To conclude, we remark that while the precise thermal flux rates and power efficiencies depend crucially on the choice of geometric configuration and materials, the system explored here is by no means optimal or unique. For instance, instead of a lattice of metal particles, one might instead consider a grating of 2d nonlinear materials<sup>41,42</sup> (e.g. graphene<sup>38,39</sup> or boron nitride<sup>40</sup>).

*Acknowledgements:* This work was partially supported by the National Science Foundation under Grant no. DMR-1454836 and by the Princeton Center for Complex Materials, a MRSEC supported by NSF Grant DMR 1420541.

- <sup>1</sup>Robert W Boyd. *Nonlinear optics*. Academic press, 2003.
- <sup>2</sup>Bahaa EA Saleh, Malvin Carl Teich, and Bahaa E Saleh. *Fundamentals of photonics*, volume 22. Wiley New York, 1991.
- <sup>3</sup>Marin Soljačić and John D Joannopoulos. Enhancement of nonlinear effects using photonic crystals. *Nature materials*, 3(4):211–219, 2004.
- <sup>4</sup>Martti Kauranen and Anatoly V Zayats. Nonlinear plasmonics. *Nature Photonics*, 6(11):737–748, 2012.
- <sup>5</sup>John D Joannopoulos, Steven G Johnson, Joshua N Winn, and Robert D Meade. *Photonic crystals: molding the flow of light*. Princeton university press, 2011.
- <sup>6</sup>MI Dykman. Theory of nonlinear nonequilibrium oscillators interacting with a medium. 1975.
- <sup>7</sup>Fardin Kheirandish, Ehsan Amooghoban, and Morteza Soltani. Finite-temperature casimir effect in the presence of nonlinear dielectrics. *Physical Review A*, 83(3):032507, 2011.
- <sup>8</sup>Chinmay Khandekar, Adi Pick, Steven G Johnson, and Alejandro W Rodriguez. Radiative heat transfer in nonlinear kerr media. *Physical Review B*, 91(11):115406, 2015.
- <sup>9</sup>Heino Soo and Matthias Krüger. Fluctuational electrodynamics for nonlinear media. *arXiv preprint arXiv:1604.05568*, 2016.
- <sup>10</sup>Chinmay Khandekar, Zin Lin, and Alejandro W Rodriguez. Thermal radiation from optically driven kerr ( $\chi$  (3)) photonic cavities. *Applied Physics Letters*, 106(15):151109, 2015.
- <sup>11</sup>S Basu, ZM Zhang, and CJ Fu. Review of near-field thermal radiation and its application to energy conversion. *International Journal of Energy Research*, 33(13):1203–1232, 2009.
- <sup>12</sup>Clayton R Otey, Wah Tung Lau, Shanhui Fan, et al. Thermal rectification through vacuum. *Physical Review Letters*, 104(15):154301, 2010.
- <sup>13</sup>Philippe Ben-Abdallah and Svend-Age Biehs. Near-field thermal transistor. *Physical review letters*, 112(4):044301, 2014.
- <sup>14</sup>Moacyr AG De Brito, Leonardo P Sampaio, Luigi G Junior, and Carlos A Canesin. Research on photovoltaics: review, trends and perspectives. In *XI Brazilian Power Electronics Conference*, pages 531–537. IEEE, 2011.
- <sup>15</sup>Yannick De Wilde, Florian Formanek, Rémi Carminati, Boris Gralak, Paul-Arthur Lemoine, Karl Joulain, Jean-Philippe Mulet, Yong Chen, and Jean-Jacques Greffet. Thermal radiation scanning tunnelling microscopy. *Nature*, 444(7120):740–743, 2006.
- <sup>16</sup>Hermann A Haus. *Waves and fields in optoelectronics*. Prentice-Hall., 1984.
- <sup>17</sup>D Ding, T Kim, and AJ Minnich. Active thermal extraction and temperature sensing of near-field thermal radiation. *Scientific Reports*, 6, 2016.
- <sup>18</sup>Chinmay Khandekar, Weiliang Jin, Owen D Miller, Adi Pick, and Alejandro W Rodriguez. Giant frequency-selective near-field energy transfer in active-passive structures. *Physical Review B*, 94(11):115402, 2016.
- <sup>19</sup>Kaifeng Chen, Parthiban Santhanam, Sunil Sandhu, Linxiao Zhu, and Shanhui Fan. Heat-flux control and solid-state cooling by regulating chemical potential of photons in near-field electromagnetic heat transfer. *Physical Review B*, 91(13):134301, 2015.
- <sup>20</sup>Ihtesham Chowdhury, Ravi Prasher, Kelly Lofgreen, Gregory Chrysler, Sridhar Narasimhan, Ravi Mahajan, David Koester, Randall Alley, and Rama Venkatasubramanian. On-chip cooling by superlattice-based thin-film thermoelectrics. *Nature Nanotechnology*, 4(4):235–238, 2009.
- <sup>21</sup>Ali Shakouri. Nanoscale thermal transport and microrefrigerators on a chip. *Proceedings of the IEEE*, 94(8):1613–1638, 2006.
- <sup>22</sup>Alejandro Rodriguez, Marin Soljačić, John D Joannopoulos, and Steven G Johnson.  $\chi$  (2) and  $\chi$  (3) harmonic generation at a critical power in inhomogeneous doubly resonant cavities. *Optics express*, 15(12):7303–7318, 2007.
- <sup>23</sup>Ioannis Karatzas and Steven Shreve. *Brownian motion and stochastic calculus*, volume 113. Springer Science & Business Media, 2012.
- <sup>24</sup>Zin Lin, Thomas Alcorn, Marko Loncar, Steven G Johnson, and Alejandro W Rodriguez. High-efficiency degenerate four-wave mixing in triply resonant nanobeam cavities. *Physical Review A*, 89(5):053839, 2014.
- <sup>25</sup>Sergei M Rytov, Yurii A Kravtsov, and Valeryan I Tatarskii. Principles of statistical radiophysics 1. 1987.
- <sup>26</sup>Craig F Bohren and Donald R Huffman. *Absorption and scattering of light by small particles*. John Wiley & Sons, 2008.
- <sup>27</sup>Alon Bahabad, Margaret M Murnane, and Henry C Kapteyn. Quasi-phase-matching of momentum and energy in nonlinear optical processes. *Nature Photonics*, 4(8):570–575, 2010.
- <sup>28</sup>Edward D Palik. *Handbook of optical constants of solids*, volume 3. Academic press, 1998.
- <sup>29</sup>Martin G Blaber, Matthew D Arnold, and Michael J Ford. Search for the ideal plasmonic nanoshell: the effects of surface scattering and alternatives to gold and silver. *The Journal of Physical Chemistry C*, 113(8):3041–3045, 2009.
- <sup>30</sup>Paul R West, Satoshi Ishii, Gururaj V Naik, Naresh K Emani, Vladimir M Shalaev, and Alexandra Boltasseva. Searching for better plasmonic materials. *Laser & Photonics Reviews*, 4(6):795–808, 2010.
- <sup>31</sup>Simon Vassant, François Marquier, Jean-Jacques Greffet, Fabrice Pardo, and Jean-Luc Pelouard. Tailoring gaas terahertz radiative properties with surface phonons polaritons. *Applied Physics Letters*, 97(16):161101, 2010.
- <sup>32</sup>JJ Wynne. Optical third-order mixing in gaas, ge, si, and inas. *Physical Review*, 178(3):1295, 1969.
- <sup>33</sup>AA Said, Mansoor Sheik-Bahae, David J Hagan, TH Wei, J Wang, James Young, and Eric W Van Stryland. Determination of bound-electronic and free-carrier nonlinearities in znse, gaas, cdte, and znte. *JOSA B*, 9(3):405–414, 1992.
- <sup>34</sup>Luis M Liz-Marzán. Tailoring surface plasmons through the morphology and assembly of metal nanoparticles. *Langmuir*, 22(1):32–41, 2006.
- <sup>35</sup>Yun Tang and Min Ouyang. Tailoring properties and functionalities of metal nanoparticles through crystallinity engineering. *Nature materials*, 6(10):754–759, 2007.
- <sup>36</sup>Hamidreza Chalabi, Erez Hasman, and Mark L Brongersma. An ab-initio coupled mode theory for near field radiative thermal transfer. *Optics express*, 22(24):30032–30046, 2014.
- <sup>37</sup>Hideo Iizuka and Shanhui Fan. Temporal coupled mode theory linking to surface-wave dispersion relations in near-field electromagnetic heat transfer. *Journal of Applied Physics*, 120(19):194301, 2016.
- <sup>38</sup>JL Cheng, Nathalie Vermeulen, and JE Sipe. Third order optical nonlinearity of graphene. *New Journal of Physics*, 16(5):053014, 2014.
- <sup>39</sup>AN Grigorenko, Marco Polini, and KS Novoselov. Graphene plasmonics. *Nature photonics*, 6(11):749–758, 2012.
- <sup>40</sup>Pathik Kumbhakar, Arup Kanti Kole, Chandra Sekhar Tiwary, Subrata Biswas, Soumya Vinod, Jaime Taha-Tijerina, Udit Chatterjee, and Pulickel M Ajayan. Nonlinear optical properties and temperature-dependent uv-vis absorption and photoluminescence emission in 2d hexagonal boron nitride nanosheets. *Advanced Optical Materials*, 3(6):828–835, 2015.
- <sup>41</sup>Han Zhang, Stéphane Virally, Qiaoliang Bao, Loh Kian Ping, Serge Massar, Nicolas Godbout, and Pascal Kockaert. Z-scan measurement of the nonlinear refractive index of graphene. *Optics letters*, 37(11):1856–1858, 2012.
- <sup>42</sup>Soo Min Kim, Allen Hsu, Min Ho Park, Sang Hoon Chae, Seok Joon Yun, Joo Song Lee, Dae-Hyun Cho, Wenjing Fang, Changgu Lee, Tomás Palacios, et al. Synthesis of large-area multilayer hexagonal boron nitride for high material performance. *Nature communications*, 6, 2015.